Abstract: Periodical switching laser pulses with nanosecond pulse width and several kilowatts peak power from wide-separated multilongitudinal-mode oscillation were observed experimentally in laser-diode pumped passively Q-switched Yb:YAG microchip laser with Cr^{4+}:YAG as saturable absorber. Pulses from different longitudinal modes oscillate alternatively. Periodical pulses oscillation dynamics induced by spatial hole burning effect and mode competition was investigated numerically by the evolution of the inversion population of different modes and the bleaching and recovery of the inversion population of the saturable absorber. The numerical simulations of switchable periodical pulsation of multilongitudinal-mode passively Q-switched Yb:YAG/Cr^{4+}:YAG microchip lasers are in good agreement with experimental results and confirmed that such pulsations are an intrinsic property in passively Q-switched Yb:YAG/Cr^{4+}:YAG microchip lasers.

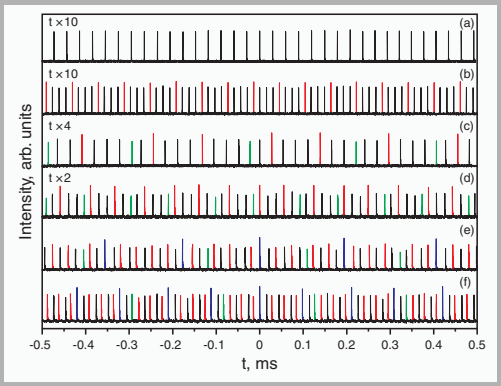

Output pulse trains of different longitudinal modes passively Q-switched Yb:YAG microchip laser under different pump power

© 2007 by Astro Ltd.
Published exclusively by WILEY-VCH Verlag GmbH & Co. KGaA

Switchable pulses generation in passively Q-switched multilongitudinal-mode microchip laser

J. Dong, * *A. Shirakawa, and K. Ueda*

Institute for Laser Science, University of Electro-Communications, 1-5-1 Chofugaoka, Chofu, Tokyo 182-8585, Japan

Received: 14 September 2006, Accepted: 18 September 2006
Published online: 9 October 2006

Key words: diode-pumped lasers; passively Q-switched; nonlinear dynamics; mode coupling; mode competition

PACS: 42.55.Xi, 42.60.Gd, 42.60.Mi, 42.65.Sf, 42.65.Pc

1. Introduction

Laser-diode (LD) end-pumped solid-state lasers are widely used as coherent light sources in optical communications, material processing. Multilongitudinal-mode operation is detrimental for the high-resolution spectroscopy that requires a narrow spectral linewidth, however, multilongitudinal-mode operation is desirable for multiplexed optical communications, material processing, industry applications that require high output power. Yttrium-aluminum-garnet (YAG) crystal doped with neodymium or ytterbium is widely used as solid-state laser medium owing to its good chemical-optical and thermal properties [1]. The number of modes m within the gain profile is given by

$$m = \Delta\nu_0 \left(\frac{c}{2nL}\right)^{-1}, \qquad (1)$$

where $\Delta\nu_0$ is the gain bandwidth, n is the refractive index, L is the cavity length, and c is the speed of light at vacuum. It is interesting to compare the number of longitudinal modes within the gain region for Nd:YAG and Yb:YAG crystals because the emission bandwidth of Yb:YAG crystal is more than ten times wider than that of Nd:YAG crystal. For Nd:YAG, $m = 2.15$ is estimated by using the parameters $\Delta\nu_0 = 177.5$ GHz, $n = 1.823$, and $L = 1$ mm. For Yb:YAG, $m = 31.59$ is estimated by using the parameters $\Delta\nu_0 = 2604$ GHz, $n = 1.823$, and $L = 1$ mm.

Therefore, single-longitudinal-mode oscillation is easier to realize by using thin Nd:YAG crystal doped with high concentration than by using Yb:YAG crystal. Multilongitudinal-mode oscillation is easier to realize by using Yb:YAG crystal as gain medium. It is still difficult to achieve single-longitudinal-mode oscillation in end-pumped Yb:YAG microchip laser ($m = 3.16$ with 100-μm

* Corresponding author: e-mail: dong@ils.uec.ac.jp

© 2007 by Astro Ltd.
Published exclusively by WILEY-VCH Verlag GmbH & Co. KGaA

thick Yb:YAG as gain medium) by reducing the thickness of the gain medium and thin gain medium is easily distorted by the pump power and also is difficult to fabricate in practice.

Although continuous-wave microchip solid-state lasers are widely used to study the nonlinear effects such as chaos, antiphase dynamics and instabilities [2–6], most of the works are done on the Nd doped gain medium. Coherent, switchable laser pulses with high peak power are required for optical communications and material processing; compact LD end-pumped passively Q-switched solid-state lasers will be potential laser sources for such applications. However, passively Q-switched pulses usually exhibit large jitters in peak power and in repetition rate that are undesirable for many applications. Pump-power-dependent pulse train bifurcation has been observed in a microchip laser [7]; however, the nonlinear dynamics of such bifurcation was not investigated in detail. Deterministic chaos of the fundamental mode oscillation [8] and the dynamics of transverse mode competition on the instabilities [9] of passively Q-switched Nd:YAG laser with Cr^{4+}:YAG saturable absorber have been reported recently. Besides the nonlinear dynamics of the fundamental mode and the transverse modes, the multilongitudinal mode competition also plays a very important role in the laser instabilities [10]. The output pulse train instabilities induced by the competition of two longitudinal-mode was observed in Cr,Nd:YAG microchip laser [10]. Owing to the narrow bandwidth of Nd in Cr,Yb:YAG crystal, only two longitudinal modes were observed. The experimental data and theoretical calculations based on the multilongitudinal-mode passively Q-switched rate equations clearly show that the instabilities induced by the longitudinal mode competition are an intrinsic properties of such passively Q-switched microchip laser. Because of the asymmetrical broad emission bandwidth of Yb:YAG crystal comparing to Nd:YAG crystal, more longitudinal modes will be observed in passively Q-switched Yb:YAG microchip lasers with Cr^{4+}:YAG as saturable absorber. The effect of longitudinal modes on the output pulse trains will be more complicated in passively Q-switched Yb:YAG microchip lasers with Cr^{4+}:YAG as saturable absorber. Stable output pulses in Cr,Yb:YAG self-Q-switched microchip multilongitudinal-mode lasers due to antiphase dynamics between longitudinal modes were achieved [11]. However, there is no such report on the effects of longitudinal mode competition and asymmetric broad gain profile on the instability or periodical pulsation of the microchip passively Q-switched solid-state lasers with a saturable absorber. In this paper, we report experimental observations of periodical switching pulses in LD-pumped passively Q-switched Yb:YAG microchip multilongitudinal-mode lasers with Cr^{4+}:YAG as saturable absorber. The pulses from different longitudinal modes oscillate in different repetition rate, the higher the longitudinal mode, the lower the repetition rate. The periodical switching pulsation of multilongitudinal-mode passively Q-switched Yb:YAG microchip lasers with Cr^{4+}:YAG as saturable absorber was also investigated theoretically by numerically solving modified multimode passively Q-switched laser rate equations. The numerical simulations of the periodical pulsation characteristics of multimode passively Q-switched lasers are in good agreement with the experimentally observed results. The dynamics of such periodical pulsation is explained by competition of the inversion population by different longitudinal modes, mode-coupling effect and nonlinear absorption of saturable absorber.

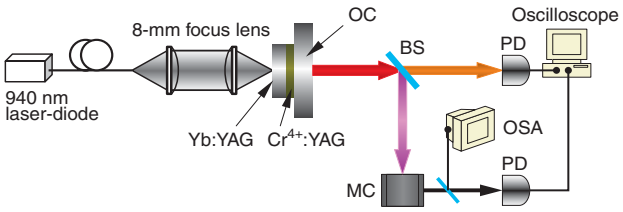

Figure 1 (online color at www.lphys.org) A schematic diagram of LD end-pumped passively Q-switched Yb:YAG microchip laser using Cr^{4+}:YAG as saturable absorber. OC, output coupler; BS, beam splitter; OSA, optical spectrum analyzer; PD, photodiode; MC, monochromator

2. Experiments

Fig. 1 shows a schematic diagram of experimental setup of passively Q-switched Yb:YAG microchip laser with Cr^{4+}:YAG as saturable absorber. An 1-mm-thick Yb:YAG crystal doped with 10 at.% Yb was used as gain medium. One surface was coated with high transmission at 940 nm and high reflection at 1.03 μm was acted as one cavity mirror, the other surface of Yb:YAG crystal was coated with high transmission at 1.03 μm and high reflection at 940 nm to increase the absorption efficiency of the pump power, and an additional advantage of this coating is the fact that the pump beam does not pass the Cr^{4+}:YAG saturable absorber, and therefore does not influence the performances of the Q-switched regime (Cr^{4+}:YAG also presents absorption at 940 nm). A 0.5-mm-thick Cr^{4+}:YAG crystal with 95% initial transmission was sandwiched between 20% transmission plane-parallel output coupler and Yb:YAG sample, which acted as a Q-switch. A high-power fiber-coupled 940 nm LD with a core diameter of 100 μm and numerical aperture of 0.22 was used as the pump source. Two lenses of 8 mm focal length were used to focus the pump beam on the crystal rear surface and to produce a pump spot in the crystal of about 100 μm in diameter. The laser spectrum was analyzed by using an optical spectrum analyzer. In order to study the pulse dynamics of different sets of modes separately, a monochromator was used as a wavelength band-pass filter to select different longitudinal modes. Pulse train of specified longitudinal-mode can be distinguished by comparing the output pulse

© 2007 by Astro Ltd.
Published exclusively by WILEY-VCH Verlag GmbH & Co. KGaA

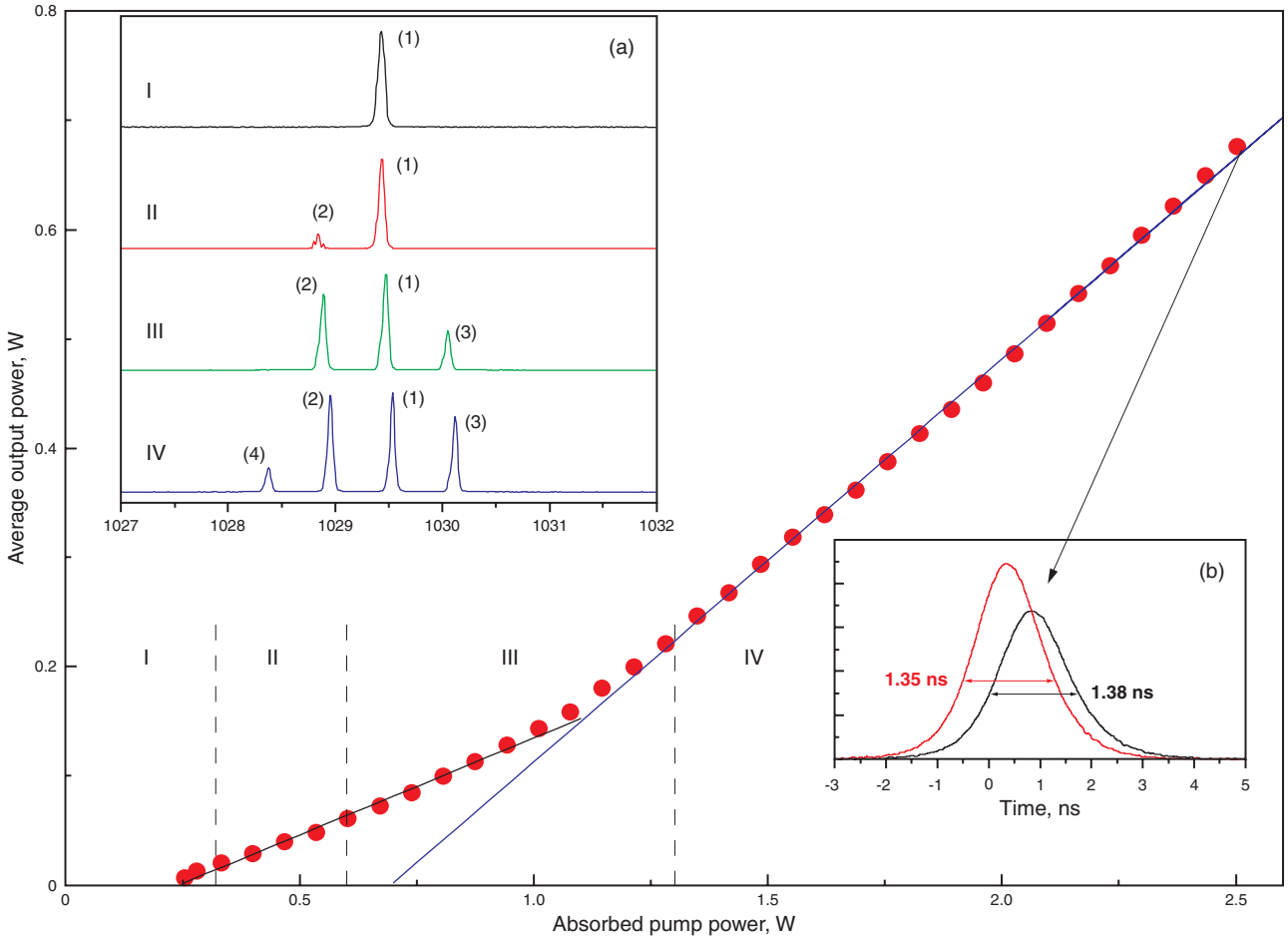

Figure 2 (online color at www.lphys.org) Average output power as a function of the absorbed pump power for passively Q-switched Yb:YAG microchip laser with Cr^{4+}:YAG as saturable absorber. The inset (a) shows the laser spectra under different longitudinal modes oscillation. The inset (b) shows the pulse profiles with high amplitude and low amplitude at absorbed pump power of 2.5 W

train of a desired mode with the total pulse train. The Q-switched pulse profiles and pulse trains were recorded by using a digital oscilloscope of 500 MHz sampling rate in the single-shot mode.

3. Experimental results

Average output power of passively Q-switched Yb:YAG/Cr^{4+}:YAG microchip laser as a function of absorbed pump power was shown in Fig. 2. The pump power threshold is about 0.25 W, and stable single-longitudinal-mode oscillation was obtained when the absorbed pump power was kept below 0.33 W. Above this value, the laser exhibited multilongitudinal-mode (up to four longitudinal modes) oscillation as shown in inset (a) of Fig. 2. Single-longitudinal-mode oscillating at $\lambda_L = 1029.4$ nm was obtained. The separation of each mode for multilongitudinal-mode oscillation, $\Delta\lambda$, was measured to be 0.58 nm, which is three times of the cavity mode space with 1.5-mm-long cavity. The wide separation of each mode for multilongitudinal-mode is attributed to the etalon effect of thin Cr^{4+}:YAG thin plate to select the preferable cavity modes [12]. The central wavelength (as indicated as 1 in the bracket in the inset (a) of Fig. 2), λ_L, shifts to longer wavelength with pump power, the side longitudinal modes prefer to oscillate at $\lambda_L - \Delta\lambda$, $\lambda_L + \Delta\lambda$, and $\lambda_L - 2\Delta\lambda$ for the second-mode, third-mode and fourth-mode, respectively. This interesting phenomenon is caused by the broad asymmetrical emission spectrum and temperature dependent emission spectrum of Yb:YAG crystal [13], the strong emission peak of Yb:YAG centered around 1.03 μm shifts to the longer wavelength with temperature. The linewidth of each mode is limited by the resolution of optical spectra analyzer, should be less than 2.83 GHz. The relative intensity of each mode changes with pump power, resulting the fluctuation of the output pulse trains. Typical pulse profiles with different amplitudes for the four-longitudinal mode oscillation at absorbed pump power of 2.5 W are also shown in the inset (b) of Fig. 2.

© 2007 by Astro Ltd.
Published exclusively by WILEY-VCH Verlag GmbH & Co. KGaA

The full width at half maximum (FWHM) difference is less than 3%. Average output power increases slowly with absorbed pump power when the absorbed pump power was lower than 1 W, the slope efficiency is about 17.7%; the slope efficiency is about 36.8% when the absorbed pump power is higher than 1 W. The change of the slope efficiency is attributed to increase of the laser modes and the pump power intensity at high pump power. The high efficiency is attributed to the high initial transmission of the Cr^{4+}:YAG saturable absorber, the slope efficiency will decrease with decrease of the initial transmission of the saturable absorber, the pulse energy will increase and pulse width will decrease with decrease of the initial transmission of the Cr^{4+}:YAG saturable absorber. There is a trade-off between efficiency and pulse energy depending on the applications of the passively Q-switched Yb:YAG microchip laser with Cr^{4+}:YAG as saturable absorber as indicated by the Q-switching theory [14,15]. A maximum average output power of 676 mW was obtained when the absorbed pump power was 2.5 W, corresponding to optical-to-optical efficiency of 27%. Pulse energy of 10.8 μJ with pulse width (FWHM) of 1.35 ns at repetition rate of 63 kHz was obtained when the absorbed pump power was 2.5 W. A maximum peak power of 8 kW was obtained. The output laser transverse intensity profile was measured by using a CCD camera in the near field and far field of the output coupler and was close to TEM_{00} mode and was near-diffraction limited with M^2 of less than 1.1. The laser beam diameter was measured to be about 90 μm, which is smaller than the pump beam diameter owing to the reabsorption of Yb:YAG at the edge of the pump beam along the radial direction.

For multilongitudinal-mode oscillation of passively Q-switched Yb:YAG/Cr^{4+}:YAG microchip lasers, the output pulses from different longitudinal modes are governed by the gain coefficient distribution for each mode, intracavity loss, and the competition of gain inside the Fabry-Perot cavity among different modes. The time interval of the total output pulse trains is determined by the bleaching and recovering of the saturable absorber, which is strongly dependent on the pump power level.

Fig. 3 shows some typical examples of the measured output pulse trains of different longitudinal modes oscillation at different absorbed pump powers. Stable single-longitudinal-mode oscillation was observed (see Fig. 3a) and pulse repetition rate was found to increase with the absorbed pump power when the absorbed pump power was above the absorbed pump power threshold, 0.25 W and was kept below 0.33 W. The laser was working in two-mode regime when the absorbed pump power was between 0.33 W and 0.6 W. The output pulse train was characterized by three pulses with nearly equal amplitudes from the first mode modulated by period–4 high amplitude pulses from second mode when the absorbed pump power was 0.5 W (see Fig. 3b). The time interval between two pulses from second mode is four times of that of total output pulse train for two longitudinal modes oscillation. Such kind of pulsation does not change with further increase

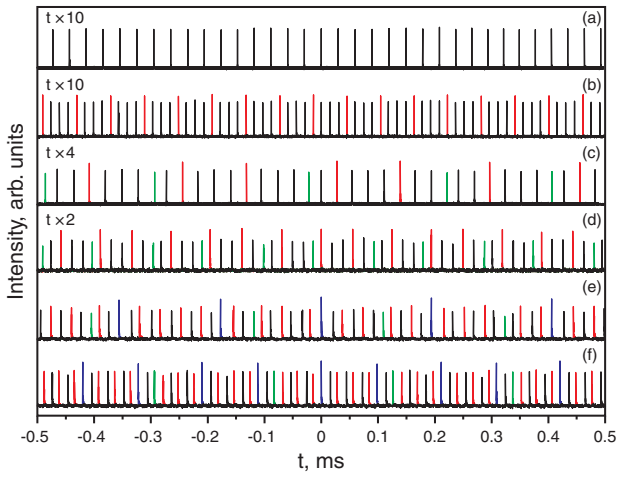

Figure 3 (online color at www.lphys.org) Output pulse trains of different longitudinal modes passively Q-switched Yb:YAG microchip laser under different pump power. (a) P_{abs} = 0.3 W; (b) P_{abs} = 0.5 W; (c) P_{abs} = 0.72 W; (d) P_{abs} = 1.2 W; (e) P_{abs} = 2.1 W; (f) P_{abs} = 2.5 W. The black, red, green and blue lines represent the pulse trains of first-mode, second-mode, third-mode and fourth-mode oscillation, respectively

of the absorbed pump power except the pulse repetition rate increases with the absorbed pump power. The same phenomenon was also observed in Cr,Nd:YAG self-Q-switched microchip lasers [10], the difference is that long time interval modulation of pulses by the second longitudinal mode in passively Q-switched Yb:YAG/Cr^{4+}:YAG microchip laser, which may be caused by the broad emission spectrum of Yb:YAG crystal comparing to the narrow emission spectrum of Nd:YAG crystal. In three-longitudinal-mode oscillation regimes when the absorbed pump power was between 0.6 W and 1.3 W, the pulse trains with low amplitude consist of pulses from the first longitudinal mode and the third longitudinal mode, the high amplitude pulses are from the second longitudinal mode oscillating at $\lambda_L - \Delta\lambda$. The output pulse trains were modulated by high amplitude pulses from second longitudinal mode and relevant amplitude pulse from third-mode with increase of the pump power, as shown in Fig. 3c and Fig. 3d. Pulses from first-mode at λ_L are dominant in the total output pulse trains. Further increase the pump power, the time interval between each pulse decreases for the total output pulse train and different modes. The time intervals between pulses for third-mode oscillating at $\lambda_L + \Delta\lambda$ is chaotic at low pump power as shown in Fig. 3c, but tend to have regular period at high pump power (see Fig. 3d). This may be caused by the strong mode competition and mode cross-saturation coupling, which strongly depend on the pump power. When the absorbed pump power was higher than 1.3 W, the laser was operating in four-longitudinal mode oscillations. The sequence of pulses from different longitudinal modes becomes com-

© 2007 by Astro Ltd.
Published exclusively by WILEY-VCH Verlag GmbH & Co. KGaA

plex, however, periodical modulation by the higher longitudinal modes still exists. The pulses with nearly equal amplitudes from first-mode at λ_L and second-mode at $\lambda_L - \Delta\lambda$ are the dominant pulses in the total output pulse trains. Alternatively switching pulses from first-mode and second-mode are modulated by the pulses from third-mode and fourth-mode with large interval time. The amplitude of pulses from third-mode is comparable to those from first-mode and second-mode. However, the amplitude of pulses form fourth-mode is higher than those from other three modes. The total output pulse trains look like periodical modulation of the pulse trains with high amplitude pulse from fourth-mode. The total pulse trains combining pulses from different longitudinal modes at different pump powers are shown in Fig. 3e and Fig. 3f. There is also repetition rate jitter between the pulses from different modes for multilongitudinal-mode oscillations. The output pulsation characteristics of this multilongitudinal-mode oscillation of passively Q-switched Yb:YAG microchip laser is caused by the cross-saturation mechanism due to the strong spatial hole burning coupling the modes via population gratings and the nonlinear absorption of the Cr^{4+}:YAG saturable absorber.

4. Theoretical modeling and discussion

For multiple longitudinal modes oscillation of passively Q-switched Yb:YAG/Cr^{4+}:YAG microchip lasers, the output pulsation of each mode is governed by the gain coefficient distribution for each mode, intracavity loss, and the competition of gain inside the Fabry-Perot cavity between each mode. The time interval of the total coherence output pulse trains is determined by the bleaching and recovering of the saturable absorber, which is strongly dependent on the pump power level. The dynamics of periodical modulation of pulse trains for the multilongitudinal-mode passively Q-switched Yb:YAG microchip laser with Cr^{4+}:YAG as saturable absorber can be described with the multimode laser rate equations by taking into account the cross-saturation dynamics that is due to the spatial hole-burning effect and the nonlinear absorption of the saturable absorber [16], as follows,

$$\frac{dn_0}{dt} = w - n_0 - \sum_{i=1}^{N} \gamma_i \left(n_0 - \frac{n_i}{2}\right) \phi_i \,, \tag{2}$$

$$\frac{dn_i}{dt} = \gamma_i n_0 \phi_i - n_i \left(1 + \sum_{j=1}^{N} C_{ij} \gamma_j \phi_j\right) , \tag{3}$$

$$\frac{d\phi_i}{dt} = K_i \left\{ \left[\gamma_i \left(n_0 - \frac{n_i}{2}\right) - 1 - \right. \right. \tag{4}$$

$$\left. \left. - \, 2 \left(\frac{\delta_1}{\gamma_i} N_g - \frac{\delta_2}{\gamma_i} (N_0 - N_g) \right) l_s \right] \phi_i + \varepsilon n_0 \right\} ,$$

$$\frac{dN_g}{dt} = (N_0 - N_g)\xi - \frac{\delta_1}{\gamma_i} N_g \sum_{i=1}^{N} \phi_i \tag{5}$$

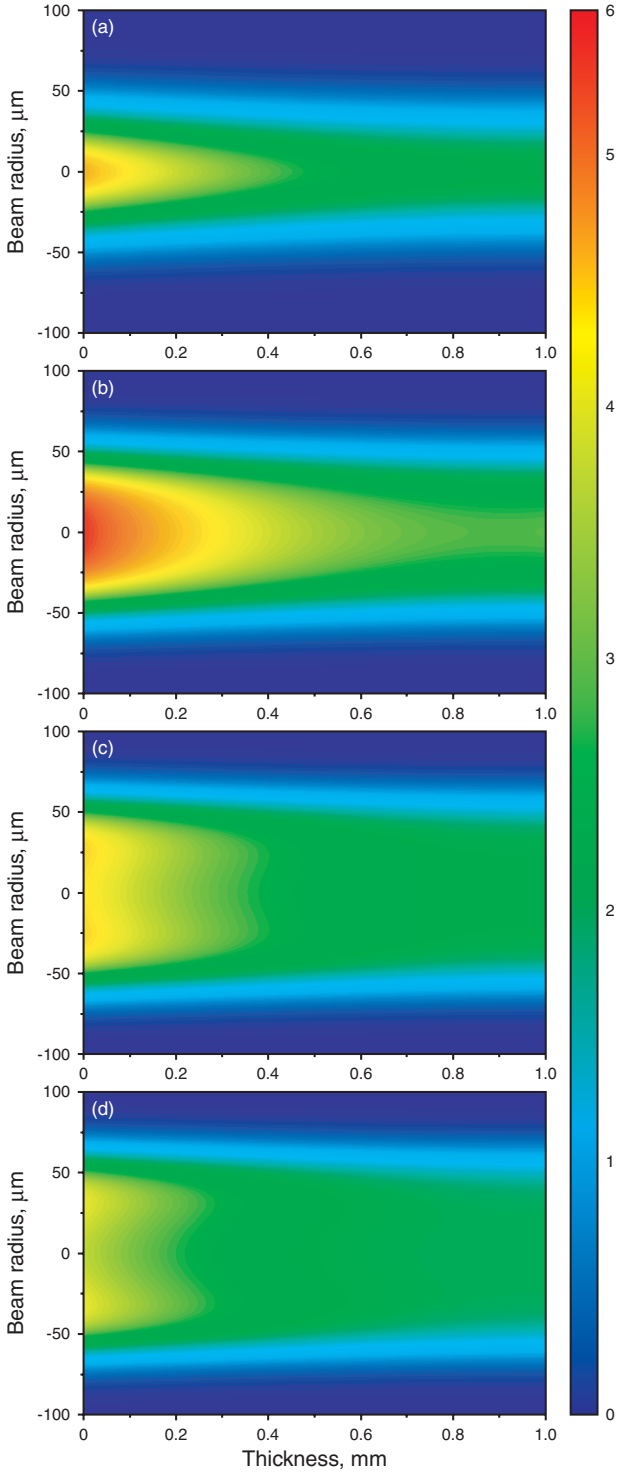

Figure 4 (online color at www.lphys.org) The variation of saturated inversion population along the thickness of 1-mm-thick Yb:YAG with beam radius under different pump powers, (a) P_{abs} = 0.3 W, (b) P_{abs} = 1 W, (c) P_{abs} = 2 W, (d) P_{abs} = 2.5 W. The unit of saturated inversion population is $\times 10^{20}$ cm^{-3}

© 2007 by Astro Ltd.
Published exclusively by WILEY-VCH Verlag GmbH & Co. KGaA

with $i = 1, \ldots, N$. In the Eqs. (2)–(5), time is normalized to the fluorescence lifetime τ of the gain medium; w is the relative pump rate normalized to the first-lasing-mode absorbed pump power threshold; n_0 and n_i are the space-averaged population inversion density and the normalized Fourier components of the population inversion density for the i-th mode normalized to the fist-lasing-mode threshold population inversion density, which can described as follows:

$$n_0 = \frac{1}{L_c} \int_0^{L_c} n(z,t) dz \,, \tag{6}$$

$$n_i = \frac{2}{L_c} \int_0^{L_c} n(z,t) \cos\left(\frac{2m_i \pi z}{L_c}\right) dz \,, \tag{7}$$

where m_i is the number of half wavelengths along the length L_c of the laser cavity axis of mode i and L_c is the length of the cavity filled with active medium; ϕ_i is the normalized photon density, $\gamma_i \leq 1$ is the relative gain with respect to the first lasing mode, $K_i = \tau/\tau_{ci}$ is the lifetime ratio of the fluorescence lifetime of the gain medium to the photon lifetime of different modes inside the laser cavity, l_s is the length of the saturable absorber, ε is the spontaneous emission coefficient, δ_1 and δ_2 are the ratio of the ground state absorption cross section and the excited state absorption cross section of Cr^{4+} saturable absorber to the stimulated emission cross section of longitudinal mode with highest gain forYb^{3+}, respectively. N_g, N_0 are the population inversion density and the total population density of Cr^{4+} saturable absorber normalized to the first-lasing-mode threshold. ξ is the ratio of the fluorescence lifetime of gain medium to the lifetime of the saturable absorber.

The cross saturation mode-coupling coefficient, C_{ij}, is a measure of the competition among the various longitudinal modes for a given inversion and is defined as an overlapping normalized integral that describes the spatial hole burning effect [17]:

$$C_{ij} = \frac{\int n(z,t) \sin^2(\theta_i) n(z,t) \sin^2(\theta_j) dz}{\int n^2(z,t) \sin^4(\theta_i) dz} \,, \tag{8}$$

where

$$\theta_{i,j} = \frac{m_{i,j} \pi z}{L} \,,$$

C_{ij} is a pump-dependent function, which results from the fact that the spatial hole-burning depth changes with the pump intensity and the variation of the inversion population under different pump power. The coupling effect among longitudinal modes will increase with the increase of the inversion population.

The oscillation of passively Q-switched Yb:YAG/Cr^{4+}:YAG microchip multilongitudinal-mode laser was determined by the initial inversion populations of passively Q-switched Yb:YAG/Cr^{4+}:YAG microchip laser and the inversion population distribution provided by the pump power. The initial inversion population of passively Q-switched Yb:YAG/Cr^{4+}:YAG microchip multilongitudinal-mode laser under continuous-wave pumping can be expressed as [15],

$$N_(i,th) = \frac{2\,\sigma_g\, N_{s0}\, l_s + \ln\left(\frac{1}{R_i}\right) + \delta_i}{2\,\sigma_i\, l} \,, \tag{9}$$

where σ_i and σ_g are the emission cross section of gain medium for different longitudinal mode, i, and the ground-state absorption cross section of Cr^{4+} saturable absorber, N_{s0} is the total concentration of Cr^{4+} in YAG, l is the length of the Yb:YAG crystal, l_s is the length of the Cr^{4+}:YAG saturable absorber, R_i is the reflectivity of the output coupler for different longitudinal mode, i, and δ_i is the total intracavity loss for different longitudinal modes. The variation of the pump power intensity on the rear surface of the gain medium with the propagation position of the pump beam can be estimated according to the expression as follows,

$$I_p(z,r) = \frac{P_{in}}{\pi\, \omega_p^2(z)} \exp\left[-\frac{2r^2}{w_p^2(z)}\right] \,, \tag{10}$$

where z is the propagation direction of the pump beam, r is the radius of the pump beam at z position, P_{in} is the incident pump power on the rear surface of the gain medium, $w_p(z)$ is the beam waist at z position of the pump beam. When the pump beam incident on the gain medium is assumed to be Gaussian beam, using a beam quality factor, M^2, the radius of the pump beam along the pump direction can be expressed as [18,19]

$$w_p^2(z) = w_{p0}^2 \left[1 + \frac{(M^2)^2\, \lambda_p^2\, (z - z_0)^2}{n^2 \pi^2 w_{p0}^4}\right] \,, \tag{11}$$

where w_{p0} is the waist of the pump beam at $z = z_0$, here z_0 is set to 0, λ_p is the pump wavelength, n is the refractive index of the gain medium. Owing to the thin gain medium used in the present passively Q-switched lasers, the variation of the pump beam diameter can be neglected, therefore, the pump beam waist can be treated as a constant along the thickness of the gain medium, i.e. $w(0) \approx w(l)$. Because of the good beam quality of laser observed the present experiment, it is still reasonable to assume that the laser beam waist is independent on the thickness of the gain medium. Therefore, w_p and w_L are used as pump beam waist and laser beam waist in the following equations.

For a microchip laser gain medium pumped by longitudinally continuous-wave incident pump power P_{in} in two-pass pumping configuration, the spatial distribution of the population inversion can be expressed as [19]

$$\Delta N(r,z) = \frac{2P_{in}\alpha f \tau}{h\nu_p \pi w_p^2} \exp\left(-\frac{2r^2}{w_p^2}\right) \times \tag{12}$$

$$\times \{\exp(-\alpha z) + \exp[-\alpha(2l - z)]\} \,,$$

© 2007 by Astro Ltd.
Published exclusively by WILEY-VCH Verlag GmbH & Co. KGaA

where r is the radial direction in the plane transverse to the laser propagation axis, z is the direction of the laser axis, h is the Planck constant, ν_p is the frequency of the pump power, τ is the fluorescence lifetime of gain medium, α is the absorption coefficient of gain medium at pump wavelength λ_p, l is the length of the gain medium, $f$is the thermal population distribution fraction of the upper laser level in the crystal field component, and w_p is the beam waist at pump beam position z. Here, the pump beam profile has been assumed to be circular and the pump beam intensity distribution is assumed to be a Gaussian profile. Therefore, the saturated inversion population can be expressed as follows,

$$N_{sat}(r,z,\lambda) = \Delta N(r,z)\left[1+\frac{I_L(r,z)}{I_{sat}(\lambda)}\right]^{-1}, \qquad (13)$$

where $I_{sat}(\lambda)$ is the laser saturation intensity of the gain medium and $I_L(r,z)$ is the intensity of the laser mode inside the cavity, $I_L(r,z)$ can be expressed as [18,19],

$$I_L(r,z) = \frac{4P_c}{\pi w_L^2}\exp\left(-\frac{2r^2}{w_L^2}\right), \qquad (14)$$

where P_c is the intracavity laser power, w_L is the intravaivty laser beam waist. The calculated saturated inversion population distribution inside 1-mm Yb:YAG crystal as a function of the thickness of the Yb:YAG crystal and beam radius under different pump powers was shown in Fig. 4. The pump beam radius and laser beam radius used in these calculations are 50 and 45 μm, respectively. The saturated inversion population inside Yb:YAG crystal decreases with the pump beam along the thickness of Yb:YAG crystal under different pump powers. The saturated inversion population distribution is wider at high pump power than that at low pump beam, and the saturated inversion population increases linearly with absorbed pump power at low pump power, and begins to decrease with further increase of the pump power at high pump power level. The variation of the inversion population distribution under different pump power will have great effect on the mode coupling coefficient, C_{ij}.

We are interested in the periodical switching pulses mechanism of multilongitudinal-mode oscillation, therefore, we focus on multilongitudinal-mode oscillation by solving the modified multi-mode rate equations of passively Q-switched Yb:YAG laser with Cr^{4+}:YAG as saturable absorber. Based on the parameters of our passively Q-switched Yb:YAG laser with Cr^{4+}:YAG as saturable absorber, we numerically solved the rate equations by using the fourth-order Runge-Kutta method. For generality, a typical numerical solution of the population inversion densities, the population inversion density of the saturable absorber, and the photon densities for four-longitudinal-mode oscillation is shown in Fig. 5. These numerical solutions of pulse repetition rate and pulse width for four-mode oscillation reproduced the experimental results shown in Fig. 3e. Numerically calculated inversion populations of different longitudinal modes vary with time and compete for the same inversion population excited by the pump power. The thresholds for different longitudinal modes increase with longitudinal mode number. Pulse will be developed when the inversion population of a certain longitudinal mode reaches its threshold firstly. The numerically calculated pulse trains also clearly show that not only the pulse amplitudes but also their pulse intervals vary periodically. The high amplitude pulses are from the side modes at short wavelengths, the shorter the wavelength, and the higher the amplitude. Although pulse amplitude from second-mode is still higher than those from first-mode and third-mode, the relative intensities are nearly the same compared to that of fourth-mode. Therefore, it looks like that the total output pulse is modulated by the

Parameters	Value
σ	2.3×10^{-20} cm^2
σ_g	4.6×10^{-18} cm^2
σ_e	8.2×10^{-19} cm^2
τ	951 μs
τ_g	3.4 μs
K	1.5×10^{7}
N_0	1.2×10^{-1}
δ_1	201
δ_2	35.6
l	1 mm
l_s	0.5 mm
ξ	280
ε	1.2×10^{-7}

Table 1 The parameters of crystal used in the numerical simulations

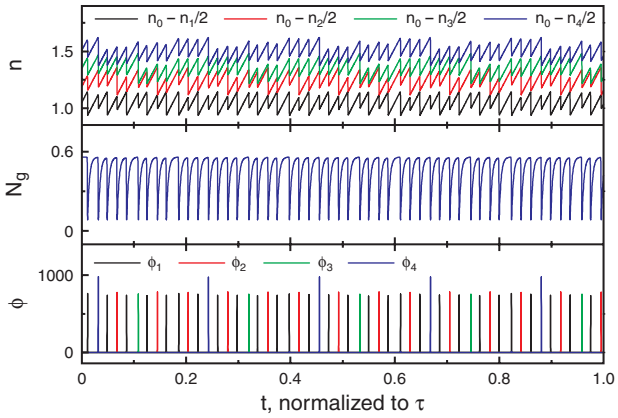

Figure 5 (online color at www.lphys.org) Numerical simulation of the population inversions of each mode, the population inversion of the saturable absorber and the photon densities for four-longitudinal-mode oscillation when the pump rate is 8.4, $\gamma_1 = 1$, $\gamma_2 = 0.98$, $\gamma_3 = 0.97$, $\gamma_4 = 0.96$. Other parameters used are listed in Table 1. The black, red, green, and blue lines represent the pulse trains of first-mode, second-mode, third-mode and fourth-mode oscillation, respectively

© 2007 by Astro Ltd.
Published exclusively by WILEY-VCH Verlag GmbH & Co. KGaA

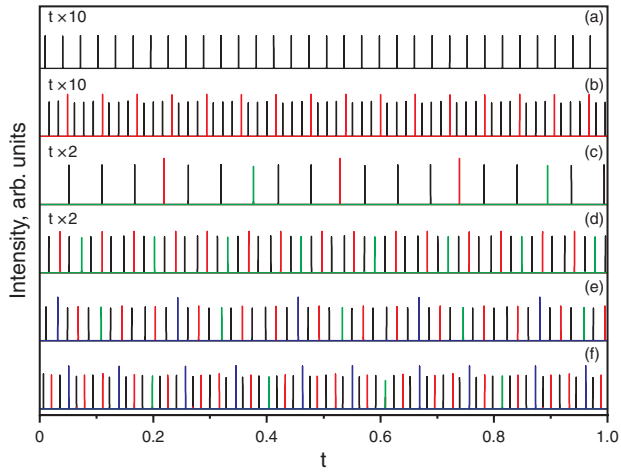

Figure 6 (online color at www.lphys.org) Passively Q-switched pulse trains as a function of the pump power ratio w obtained by numerically calculations of the modified rate equations. (a) $w = 1.2$, (b) $w = 2$, (c) $w = 2.9$, (d) $w = 4.8$, (e) $w = 8.4$, (f) $w = 10$. The black, red, green, and blue lines represent the pulse trains of first-mode, second-mode, third-mode and fourth-mode oscillation, respectively

pulses with high amplitude. Pulse width (FWHM) difference from such two kinds of pulses with different amplitudes is less than 2%, which is in good agreement with the experimental data (inset (b) of Fig. 2). Fig. 6 shows the numerical simulations of periodical pulse trains of different longitudinal modes oscillation under different pump rate, which reproduce experimental observed pulse trains for different longitudinal modes oscillation. The discrepancies between observed periodical pulsation and numerical simulation (see Fig. 3 and Fig. 6) are attributed to some uncertainties in the determination of the mode-coupling coefficients, the gain profile under lasing and pumping for quasi-three level Yb:YAG system. The thermal effect in Yb:YAG gain medium also plays a very important role on the laser performance, the thermal population distribution will be affected strongly by pump power, however, this thermal effect is not taken into account in our model.

5. Conclusions

In conclusion, periodical switchable pulses were observed experimentally in passively Q-switched Yb:YAG microchip multilongitudinal-mode laser with Cr^{4+}:YAG as saturable absorber. Stable single-longitudinal-mode oscillation and wide-separated multilongitudinal-mode oscillation in passively Q-switched Yb:YAG microchip lasers with Cr^{4+}:YAG as saturable absorber was attributed to the spatial hole burning effect in Yb:YAG gain medium and the mode section of Cr^{4+}:YAG etalon. The periodical pulsation of multi-mode oscillation was caused by the spatial hole burning effect and mode competition effect. The numerical simulation based on the multilongitudinal-mode passively Q-switched laser rate equations almost reproduces the observed periodical pulsation of multi-mode oscillation and confirms that the periodic pulsation dynamics of passively Q-switched Yb:YAG microchip lasers with Cr^{4+}:YAG as saturable absorber is an intrinsic property of such laser. Such kinds of periodical switching pulses of multilongitudinal-mode oscillation in passively Q-switched Yb:YAG microchip laser with Cr^{4+}:YAG as saturable absorber can be controlled by using Cr^{4+}:YAG crystals with different Cr^{4+} concentrations and different thickness, and varying the pump power incident on the Yb:YAG crystal. Each pulse corresponds to a specified longitudinal mode at certain wavelength. Such compact multi-wavelength solid-state laser pulses with high peak power will be potential sources for wavelength division multiplex (WDM) or frequency division multiplex (FDM) in optical communications.

Acknowledgements This work was supported by the 21st Century Center of Excellence (COE) program of Ministry of Education, Science, Sports and Culture of Japan.

References

[1] W.F. Krupke, IEEE J. Sel. Top. Quantum Electron. **6**, 1287 (2000).
[2] K. Otsuka, Y. Asakawa, R. Kawai, S. Hwong, and J. Chern, Jpn. J. Appl. Phys. **37**, L1523 (1998).
[3] K. Otsuka, S. Hwong, and B. Nguyen, Phys. Rev. A **61**, 053815 (2000).
[4] K. Otsuka, J. Ko, T. Kubota, S. Hwong, T. Lim, J. Chern, B. Nguyen, and P. Mandel, Opt. Lett. **26**, 1060 (2001).
[5] K. Otsuka, Phys. Rev. Lett. **67**, 1090 (1991).
[6] M.A. Larotonda, A.M. Yacomotti, and O.E. Martinez, Opt. Commun. **169**, 149 (1999).
[7] J.J. Zayhowski and C. Dill-III, Opt. Lett. **19**, 1427 (1994).
[8] D.Y. Tang, S.P. Ng, L.J. Qin, and X.L. Meng, Opt. Lett. **28**, 325 (2003).
[9] M. Wei, C. Chen, and K. Tu, Opt. Express **12**, 3972 (2004).
[10] J. Dong and K. Ueda, Appl. Phys. Lett. **87**, 151102 (2005).
[11] J. Dong, A. Shirakawa, S. Huang, Y. Feng, T. Takaichi, M. Musha, K. Ueda, and A.A. Kaminskii, Laser Phys. Lett. **2**, 387 (2005).
[12] J. Dong, A. Shirakawa, and K. Ueda, Appl. Phys. B, in press (2006).
[13] J. Dong, M. Bass, Y. Mao, P. Deng, and F. Gan, J. Opt. Soc. Am. B **20**, 1975 (2003).
[14] J.J. Degnan, IEEE J. Quantum Electron. **25**, 214 (1989).
[15] J.J. Degnan, IEEE J. Quantum Electron. **31**, 1890 (1995).
[16] C.L. Tang, H. Statz, and G. Demars, J. Appl. Phys. **34**, 2289 (1963).
[17] E. Lacot and F. Stoeckel, J. Opt. Soc. Am. B **13**, 2034 (1996).
[18] T. Taira, J. Saikawa, T. Kobayashi, and R.L. Byer, IEEE J. Sel. Top. Quantum Electron. **3**, 100 (1997).
[19] J. Dong and K. Ueda, Laser Phys. Lett. **2**, 429 (2005).

© 2007 by Astro Ltd.
Published exclusively by WILEY-VCH Verlag GmbH & Co. KGaA